# Exceptional Tunability of Band Energy in a Compressively Strained Trilayer $MoS_2$ Sheet

Yeung Yu Hui,[†,⊥] Xiaofei Liu,[‡,⊥] Wenjing Jie,[†] Ngai Yui Chan,[†] Jianhua Hao,[†] Yu-Te Hsu,[§] Lain-Jong Li,[§] Wanlin Guo,[‡,*] and Shu Ping Lau[†,*]

[†]Department of Applied Physics and Materials Research Centre, The Hong Kong Polytechnic University, Hung Hom, Kowloon, Hong Kong SAR, China, [‡]State Key Laboratory of Mechanics and Control of Mechanical Structures, Key Laboratory for Intelligent Nano Materials and Devices of Ministry of Education and Institute of Nano Science, Nanjing University of Aeronautics and Astronautics, Nanjing 210016, China, and [§]Institute of Atomic and Molecular Sciences, Academia Sinica, Taipei 10617, Taiwan. [⊥]Y. Y. Hui and X. Liu contributed equally to this work.

**ABSTRACT**

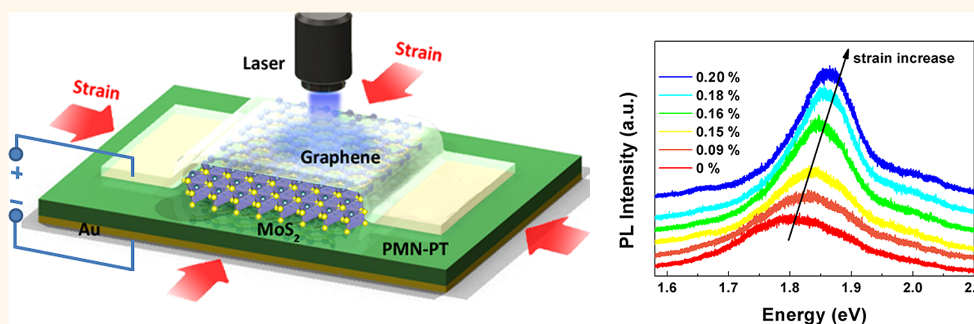


Tuning band energies of semiconductors through strain engineering can significantly enhance their electronic, photonic, and spintronic performances. Although low-dimensional nanostructures are relatively flexible, the reported tunability of the band gap is within 100 meV per 1% strain. It is also challenging to control strains in atomically thin semiconductors precisely and monitor the optical and phonon properties simultaneously. Here, we developed an electromechanical device that can apply biaxial compressive strain to trilayer $MoS_2$ supported by a piezoelectric substrate and covered by a transparent graphene electrode. Photoluminescence and Raman characterizations show that the direct band gap can be blue-shifted for ~300 meV per 1% strain. First-principles investigations confirm the blue-shift of the direct band gap and reveal a higher tunability of the indirect band gap than the direct one. The exceptionally high strain tunability of the electronic structure in $MoS_2$ promising a wide range of applications in functional nanodevices and the developed methodology should be generally applicable for two-dimensional semiconductors.

**KEYWORDS:** $MoS_2$ · strain engineering · piezoelectric substrate · Raman spectroscopy · photoluminescence

Strain engineering is a powerful and widely used strategy for boosting the performance of electronic, optoelectronic, and spintronic devices.[1−4] By applying a strain through lattice mismatch between epitaxial films and substrates or through bending of films on elastic substrates, this strategy can be used to increase the carrier mobility in semiconductors[1] or to raise the emission efficiency of light-emitting devices.[4] Particularly, due to reduced dimensions, nanostructures become more flexible to be highly strained, which provides more space for strain engineering. A vast array of strain effects on the electronic behaviors in quasi one-dimensional nanostructures such as carbon nanotubes, GaAs nanowires, and ZnO nanowires have been revealed.[5,6] Technically speaking, the emerging two-dimensional (2D) crystals such as graphene, hexagonal boron nitride, and molybdenum disulfide ($MoS_2$) are more favored for strain engineering,[7] as they are only one or a few atoms in thickness. Whereas the strain-tunable phonon properties in graphene are intensively studied by Raman scattering, the theoretically predicted bandgap opening in graphene by strain has not been achieved in experiments.[7−9] On the other hand, 2D atomic layers of $MoS_2$, one of

* Address correspondence to apsplau@polyu.edu.hk, wlguo@nuaa.edu.cn.

Received for review May 16, 2013 and accepted July 11, 2013.

Published online July 11, 2013
10.1021/nn4024834

© 2013 American Chemical Society



ARTICLE

transition metal dichalcogenides, have attracted great interest because of their distinctive electronic and optical properties; especially their band gap has been predicted to be highly strain-tunable.[10,11] Hence, developing effective routes to apply tunable strain in 2D atomic layers such as $MoS_2$ is highly desirable for strain engineering.

Here, we develop a novel electromechanical device to apply uniform and controllable biaxial compressive strain up to 0.2% in trilayer $MoS_2$ and perform photoluminescence (PL) and Raman detections simultaneously. The strain is applied by a piezoelectric substrate, while its transparency to PL detection is realized by using a graphene layer as transparent top electrode. The PL and Raman spectra measurements show that the electronic structure and phonon spectrum in trilayer $MoS_2$ can be smoothly modulated by strain ranging from 0 to 0.2%, which is further confirmed by first-principles investigations. Surprisingly, the direct band gap of trilayer $MoS_2$ blue-shifts remarkably by ~300 meV per 1% strain, which is unprecedentedly large among all bulk or nanostructure semiconductors under strain. Moreover, the PL intensity can be increased by 200% accompanied with a ~40% reduction in the full-width at half-maximum (fwhm) of the emission spectrum for an applied strain of ~0.2%. These results build up a platform generally applicable for strain engineering in emerging 2D crystals such as transition metal dichalcogenides.

## RESULTS AND DISCUSSION

Figure 1 depicts the configuration of our electromechanical device. The starting point for the fabrication of our electromechanical device was the chemical vapor deposition (CVD) of large-area trilayer $MoS_2$.[12] The number of layers was clearly identified from the high-resolution transmission electron microscopy (TEM) image at the edge of the $MoS_2$ sample (Figure 1b) and verified by atomic force microscopy (AFM) with a thickness of ~2.1 nm (Figure 1c). Then, the $MoS_2$ sample was transferred onto a piezoelectric substrate ($[Pb(Mg_{1/3}Nb_{2/3})O_3]_{0.7}$-$[PbTiO_3]_{0.3}$, PMN-PT) and covered by a monolayer of graphene as the top electrode. When a bias voltage was applied between the graphene top electrode and the gold bottom electrode, a biaxial compressive strain can be applied to the substrate due to piezoelectricity[13] and then transferred to the trilayer $MoS_2$. In our experiments, the PMN-PT was not polarized before the measurement, which guarantees that the PMN-PT can generate only an in-plane compressive stress regardless of the bias voltage directions. Indeed we obtained nearly the same results when the polarity was reversed in our experiments. It is worth mentioning that the top graphene electrode is essential for the electromechanical device. First, while graphene is conductive as an electrode, it is transparent without blocking the PL and Raman signal from the

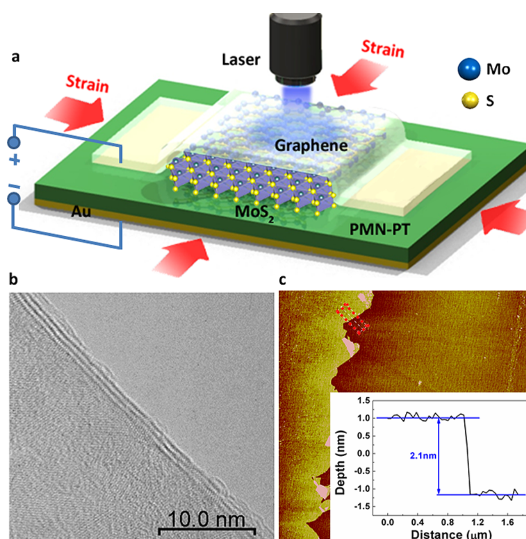


**Figure 1. Experimental setup and structural properties of trilayer $MoS_2$. (a) Schematic diagram of Raman and PL measurements on $MoS_2$ that is sandwiched between a piezoelectric PMN-PT substrate and a graphene top electrode. (b) High-resolution TEM image at the edge of trilayer $MoS_2$. (c) AFM image of the trilayer $MoS_2$. The inset shows the depth profile of the trilayer $MoS_2$, which indicates a thickness of 2.1 nm.**

$MoS_2$. Second, the atomically thin graphene is relatively soft compared with other conductive films as an electrode. As a result, the strain from the substrate can be fully transferred to the $MoS_2$ sheet without being blocked by other thick electrodes. Another advantage of this device structure is that the resistances of the monolayer graphene (~kΩ) and the trilayer $MoS_2$ (~MΩ) were low as compared with the insulating PMN-PT substrate (~GΩ) such that the voltage drop from the intermediate $MoS_2$ or graphene sheets can be neglected.

The polarization-induced strain in the lattices of piezoelectric substrate and trilayer $MoS_2$ was probed by X-ray diffraction (XRD) measurement (Supporting Information, Figures S1 and S2). As the vertical voltage increased, the XRD peak that corresponds to the (002) plane (*i.e.*, *c*-axis) of the PMN-PT substrate shifted to lower angles,[14] which indicated that the out-of-plane lattice constant *c* and the in-plane lattice constant in the substrate were expanding and shrinking, respectively. The relation[15] between the polarization-induced out-of-plane strain $\varepsilon_\perp$ and in-plane strain $\varepsilon_\parallel$ in the PMN-PT substrate can be written as $\varepsilon_\parallel \approx -0.7\varepsilon_\perp$. When the biased voltage reached 500 V (*i.e.*, 10 kV/cm), the in-plane compressive strain was estimated to be about 0.2%. In the case of $MoS_2$, the characteristic XRD peak of the $MoS_2$ (*i.e.*, (105)) also shifted to lower angles compared with that in the strain-free status, which implied that the compressive strain was transferred from the PMN-PT to the $MoS_2$. However, it was not possible to estimate the strain magnitude induced in the $MoS_2$ sheet directly by its XRD characterization,

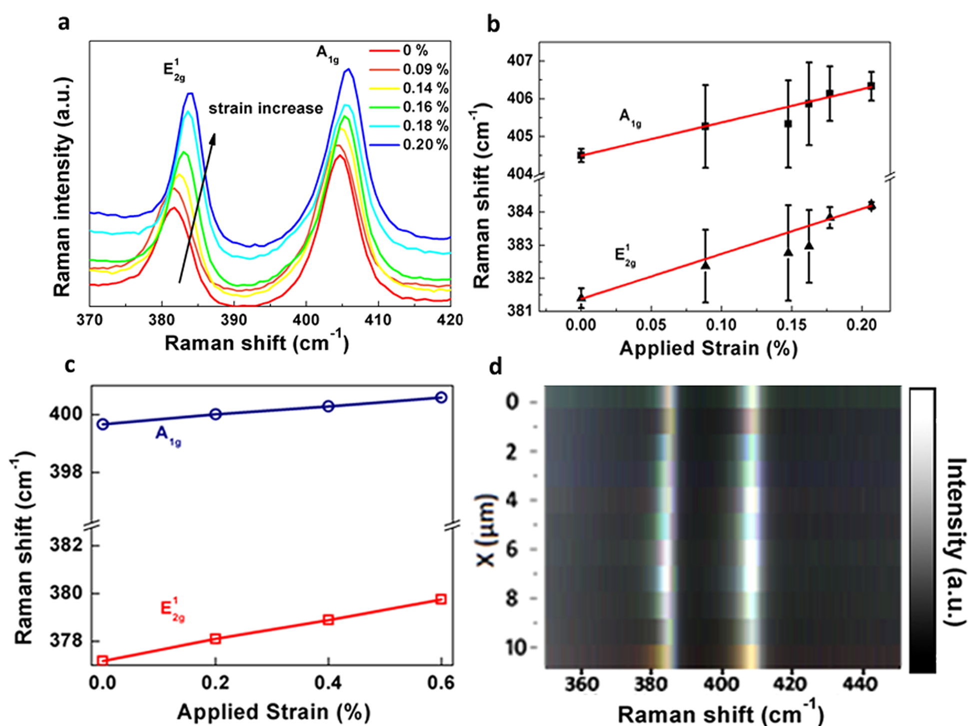


Figure 2. Raman spectra of trilayer $MoS_2$ under different strains. (a) Raman spectra of the trilayer $MoS_2$ under various applied strains. (b) Raman shift of the $E^1_{2g}$ and $A_{1g}$ modes as a function of strain. (c) Raman shift of the the $E^1_{2g}$ and $A_{1g}$ modes as a function of strain calculated by density functional perturbation theory. (d) 1D spatial mapping of the Raman shift of $E^1_{2g}$ and $A_{1g}$ modes under the applied strain of 0.2%.

since we could observe only one prominent (105) peak. Although it is still unclear whether the interfacial mechanic interaction is strong enough to completely transfer the strain produced in the PMN-PT to the target $MoS_2$, for simplicity, the strain value in the trilayer $MoS_2$ is assumed to be equal to the strain measured from the PMN-PT.

Figure 2a presents the typical Raman spectra of the $MoS_2$ at different strains. Among the four Raman-active modes of bulk $MoS_2$, the $E^1_{2g}$ and $A_{1g}$ modes for the strain-free trilayer $MoS_2$ were observed at 382.4 and 405.4 $cm^{-1}$, respectively. The difference between the two modes is 23 $cm^{-1}$, in good agreement with that found in mechanically exfoliated trilayer $MoS_2$.[16,17] Both of the modes shifted to higher frequencies (Figure 2b) as compressive strain was applied. For the applied strain of 0.2%, the $E^1_{2g}$ and $A_{1g}$ modes shifted by ~3 and ~2 $cm^{-1}$, respectively, with a shift ratio of $E^1_{2g}$ to $A_{1g}$ of ~1.5. Since the blue-shift of the two modes was previously observed in $MoS_2$ nanotubes and $MoS_2$ bulk crystal at high pressure,[18,19] the observed change in the Raman modes was surely attributed to the presence of compressive strain. To further confirm this, we calculated the responses of Raman modes at strains ranging from 0.0 to 0.6% (Figure 2c). The calculated Raman modes exhibit a similar trend of blue-shifts to those observed in the experiment, but with a higher Raman shift ratio of $E^1_{2g}$ to $A_{1g}$ of ~2.5. In general, the calculated Raman frequencies were underestimated (Supporting Information, Table SI), but the deviation from experiments was only a few $cm^{-1}$. Likely, the calculated blue-shift rates in trilayer $MoS_2$ were also underestimated such that the blue-shifts for $E^1_{2g}$ and $A_{1g}$ were ~0.93 and ~0.35 $cm^{-1}$ at 0.2% strain, respectively.

The evolution of the electronic structure in the trilayer $MoS_2$ under biaxial compressive strain was investigated by PL spectroscopy. At the strain-free state, a broad PL peak centered at 1.8 eV was observed, which can be assigned to the direct band emission ($E_{dir}$) of $MoS_2$.[12,20,21] As the strain increased, the PL emission peak shifted to higher energy remarkably and near linearly, and a total shift of ~60 meV (~20 nm change in wavelength) was recorded with an applied strain of 0.2% (Figure 3b). Upon slow release of the strain, the PL peak could return to the original position approximately following the original path even after several cycles of repeated measurements (Supporting Information, Figure S3). Therefore, the strain transferred into the trilayer $MoS_2$ was in its elastic region and fully controlled by the electromechanical device. In addition to the effective control of the $E_{dir}$, an increase of the PL emission intensity up to ~200% and a reduction of fwhm by 40% were observed (see the inset in Figure 3b and Supporting Information, Figure S4). The increase in PL intensity indicates the enhancement of light emission efficiency. The applied strain modifies the band structure of the $MoS_2$ and in turn increases the density of states of the carriers. Due to the increase in carrier population, the radiative

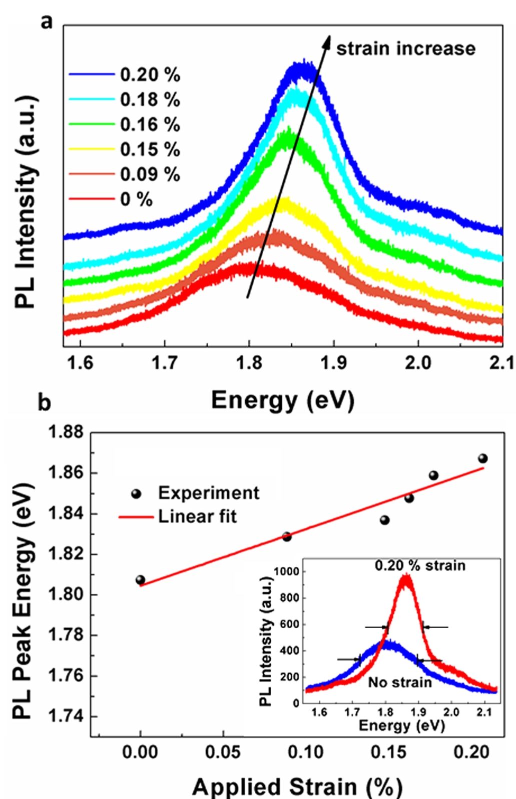


**Figure 3. Photoluminescence property of trilayer $MoS_2$ under strain. (a) PL spectra of the $MoS_2$ under various strains. (b) PL peak energy as a function of compressive strain. The inset shows PL spectra of the sample under 0.0% and 0.2% strain.**

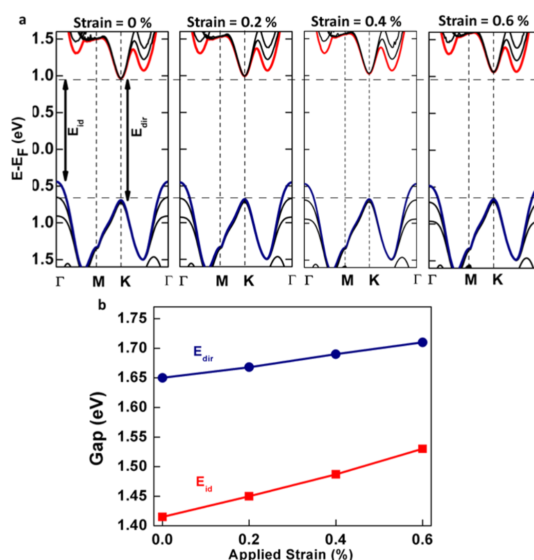


**Figure 4. First-principles band structures of trilayer $MoS_2$. (a) Band structures of *AbA-BaB* stacking trilayer $MoS_2$ under 0.0%, 0.2%, 0.4%, and 0.6% biaxial compressive strain. (b) Energy gaps as a function of biaxial compressive strain.**

recombination of carriers increases, which leads to an increase in PL intensity. It is worth noting that the tunability of $E_{dir}$ by strain is ~300 meV per 1% strain, which is the highest value ever reported for strained semiconductors to the best of our knowledge. For instance, band-gap tunability in semiconductors, such as GaAs/AlGaAs quantum dots[15] (~70 meV/%), GaAs nanowires[5] (~85 meV/%), and ZnO nanowires[22] (~35 meV/%), were reported.

To understand the strain dependence of the PL spectra, we carried out first-principles calculations for band structures of trilayer $MoS_2$ under different biaxial strains. Consistent with pervious research, trilayer $MoS_2$ is shown to be an indirect semiconductor,[23] with an indirect band gap ($E_{id}$) determined by the valence band maximum (VBM) at the Γ point and the conduction band minimum (CBM) at the K point. Although the first-principles calculations usually underestimate the band gaps, the trend of change in $E_{dir}$ under applied strain agrees with the PL emission peak shifts. According to our calculation and previous studies,[24,25] the CBM at the K point from both Mo $d_{xy}-d_{x^2-y^2}$ and $d_{z^2}$ states is of an antibonding nature and, thus, can be increased in energy when the in-plane lattice is compressed. In contrast, the VBM at the Γ point also has an antibonding nature but is composed of Mo $d_{z^2}$ and S $p_z$ orbitals, which can induce a decrease in energy as the out-of-plane component of Mo–S bond is stretched upon in-plane compression due to the Poisson effect. Indeed we observed that, under increasing compressive strain, the CBM at the K point and the VBM at the Γ point shift to higher and lower energies, respectively.

As shown in Figure 4a, with increased compressive strain, both VBM and CBM shift to higher energies, but the CBM is more sensitive to strain, resulting in an enlargement of $E_{dir}$. At an applied strain of 0.2%, the calculated blue-shifts of $E_{dir}$ and $E_{id}$ are 18 and 36 meV, respectively, severely underestimated as compared with the experimentally observed shift for $E_{dir}$ (~60 meV). The computational results also imply that the trilayer $MoS_2$ remains an indirect semiconductor under compressive strain up to 0.6%, but the energy difference between $E_{id}$ and $E_{dir}$ is reduced as the strain increases (Figure 4b). Moreover, the strain-tunability of $E_{id}$ in trilayer $MoS_2$ is twice the value of $E_{dir}$ according to the first-principles results (Supporting Information, Table S2). It is noteworthy that there are two possible stacking sequences for trilayer $MoS_2$, namely, *AbA-AbA* and *AbA-BaB* (Supporting Information, Figure S5), and the above band structures are results from *AbA-BaB* stacking $MoS_2$. While the band gaps of *AbA-AbA* stacking $MoS_2$ are slightly larger, the trend of the band gaps under strain is the same. The above band structure calculations do not take into consideration the spin–orbit coupling since the spin–orbit interactions arise from the inner parts of the atoms and are insensitive to the atomic bond lengths.[26]

It is of significance that the observed strain-induced shift of band energy in our experiment was from a large-area and homogeneous trilayer $MoS_2$ rather than from a nonuniform $MoS_2$ with a mixture of number of layers, which usually happens in mechanically

exfoliated $MoS_2$ sheets. To verify that our sample contained only uniform trilayer $MoS_2$, we measured the PL and Raman mappings of the sample. The typical mapping results showed that over a $10 \times 10\ \mu m^2$ scanning area the PL and Raman peak intensities were uniform and the positions of the two Raman modes were constant in the entire scanning area on their respective frequencies (Supporting Information, Figure S6). More importantly, we found that the applied strain was also uniform and homogeneous, which was clearly shown by the 1D spatial Raman mapping of the $MoS_2$ under a strain of 0.2% in Figure 2d. In our device, only biaxial compressive strain can be applied to the trilayer $MoS_2$. However, in principle, biaxial tensile strain can also be achieved by a piezoelectric substrate,[15] which can not only tune the band gap but also reduce the carrier effective masses.[24,27] Recently, the band-gap reduction was observed from mechanically exfoliated monolayer and bilayer $MoS_2$ nanosheets deposited on an elastic substrate when tensile strain is applied by bending the substrate.[26,28] It is noted that the sensitivity of band-gap shift per % strain is much higher for biaxial strained $MoS_2$ as compared to tensile strain (Supporting Information, Table SIII). This observation is understandable because the bonds are compressed only along one direction under the uniaxial strain.

Finally, we can rule out the possibility that the band structures of the trilayer $MoS_2$ could be influenced by the applied vertical electric field, considering that the band gap of bilayer $MoS_2$ could be reduced only by a field 4 orders of magnitude larger than that used in our device.[29] Furthermore, when we replaced the piezoelectric PMN-PT substrate with a sapphire substrate, no PL or Raman shifts in the trilayer $MoS_2$ were observed under the same field strength.

## CONCLUSIONS

In summary, the experimental approach demonstrated here is based on the use of piezoelectric actuators made of single-crystal PMN-PT, which are capable of providing controllable compressive strain up to 0.2%. In addition to the ability to tune the emission energy over a large range of 60 meV, the applied strain can enhance the PL intensity. The developed methodology can be employed on a wide range of 2D crystals. Besides the band structure, it will also allow us to investigate in detail the effects produced by tunable strains on other important physical properties of 2D crystals such as ferromagnetism.[30,31] We envision its use in high-performance electronic, piezoelectric, photovoltaic, optoelectronic, and spintronic devices.

## METHODS

**Fabrication of the Electromechanical Device.** The PMN-PT substrates were obtained from Heifei Kejing Materials Technology Company. Large-area and highly crystalline trilayer $MoS_2$ ($1 \times 1\ cm^2$) was grown by CVD on a sapphire substrate using a technique described by Liu *et al.*[12] In order to transfer the as-grown $MoS_2$ onto the PMN-PT ($7 \times 7$ mm and 0.5 mm thick), the $MoS_2$ was coated with a layer of PMMA (Micro Chem. 950K A4) by spin-coating (step 1: 500 rpm for 10 s; step 2: 3000 rpm for 60 s), followed by baking at 100 °C for 10 min. After that, the PMMA-capped $MoS_2$ was then put into a NaOH (2 M) solution at 100 °C for 30 min. The PMMA-capped $MoS_2$ film was transferred to deionized (DI) water to dilute and remove the etchant and residues. A PMN-PT substrate treated with $O_2$ plasma for 5 min was then used to lift the PMMA-capped $MoS_2$ film, followed by drying on a hot-plate (100 °C for 10 min). The PMMA was removed by acetone, isopropyl alcohol, and then DI water. After that, chloroform was used to further clean the $MoS_2$ surfaces. CVD-grown monolayer graphene was then transferred on top of the $MoS_2$ from copper foil using a similar method, while the copper foil was etched by iron chloride ($FeCl_3$). The bottom Au electrode (~100 nm thick) was deposited by sputtering with a current of 80 mA and pressure of $\sim 10^{-2}$ Torr after the flow of Ar gas. The four edges of the PMN-PT substrate were masked to avoid short-circuit between the top and bottom electrode. A wire bonder was used to connect an electrical wire from the top graphene electrode to a printed circuit board for electrical connection (see Figure S7).

**Characterizations.** The AFM measurements were performed in a Veeco Dimension-Icon system. A scanning rate of 0.972 Hz with 512 scanning lines was used. Raman spectra were collected in a Horiba Jobin Yvon HR800 Raman microscopic system. The solid-state excitation laser has a wavelength of 488 nm and a spot size of ~1 $\mu$m with a power of 180 mW. A 100× objective lens with a numerical aperture of 0.9 was used in the measurement at room temperature. A Si sample with a feature peak at 520.5 $cm^{-1}$ was used as a reference for wavenumber calibration in the Raman and photoluminescence characterization. The PL measurements were also performed with the same laser using the PL mode of the Raman microscopic system. The data acquisition time of the Raman and PL spectra was set to 20 s. A high-resolution X-ray diffractometer (Rigaku, SmartLab, 9 kW) equipped with a Ge (220) 2 bounce monochromator was used to obtain $2\theta$ scanning patterns of the single-crystal PMN-PT substrate. The structure of the $MoS_2$ sheets was characterized by a JEOL-2010F TEM with an accelerating voltage of 200 keV. The electrical measurements were performed in ambient conditions using a Keithley 2410 SourceMeter to provide a dc voltage for the graphene/$MoS_2$/PMN-PT electromechanical device.

**First-Principles Calculations.** The first-principles calculations for the band structure of trilayer $MoS_2$ was performed within the framework of density functional theory as implemented in the VASP code.[32,33] The projector-augmented wave method[34,35] for the core region and the Perdew–Burke–Ernzerhof functional[36] for the exchange–correlation potential were employed in calculations. The kinetic energy cutoff of the plane-wave expansion is set at 500 eV. The conjugate gradient method was used to fully relax the geometry until the force on each atom is less than 0.01 eV/Å. Convergence with respect to the mesh of K points was carefully tested before the calculations. The calculations of Raman modes were performed with density functional perturbation theory.[37]

*Conflict of Interest:* The authors declare no competing financial interest.

*Acknowledgment.* This work was financially supported by the Research Grants Council of Hong Kong (Project No. PolyU 5006/12P) and HK PolyU Grant (Project No. 1-ZV8N). W.G. thanks the 973 Programs (2013CB932604, 2012CB933403) and NSF of China (91023026) for financial support.

*Supporting Information Available:* XRD of the PMN-PT and $MoS_2$, elasticity of the $MoS_2$, Raman and PL mappings, and calculated Raman frequencies and band-gap energies. This

material is available free of charge *via* the Internet at http://pubs.acs.org.

## REFERENCES AND NOTES


1. Fischetti, M. V.; Laux, S. E. Band Structure, Deformation Potentials, and Carrier Mobility in Strained Si, Ge, and SiGe Alloys. *J. Appl. Phys.* **1996**, *80*, 2234–2252.
2. Feng, J.; Qian, X.; Huang, C. W.; Li, J. Strain-Engineered Artificial Atom as a Broad-Spectrum Solar Energy Funnel. *Nature Photon* **2012**, *6*, 866–872.
3. Kato, Y.; Myers, R. C.; Gossard, A. C.; Awschalom, D. D. Coherent Spin Manipulation without Magnetic Fields in Strained Semiconductors. *Nature* **2004**, *427*, 50–53.
4. Yang, Q.; Wang, W. H.; Xu, S.; Wang, Z. L. Enhancing Light Emission of ZnO Microwire-Based Diodes by Piezo-Phototronic Effect. *Nano Lett.* **2011**, *11*, 4012–4017.
5. Signorello, G.; Karg, S.; Björk, M. T.; Gotsmann, B.; Riel, H. Tuning the Light Emission from GaAs Nanowires over 290 meV with Uniaxial Strain. *Nano Lett.* **2013**, *13*, 917–924.
6. Wei, B.; Zheng, K.; Ji, Y.; Zhang, Y.; Zhang, Z.; Han, X. Size-Dependent Bandgap Modulation of ZnO Nanowires by Tensile Strain. *Nano Lett.* **2012**, *12*, 4595–4599.
7. Lee, C.; Wei, X.; Kysar, J. W.; Hone, J. Measurement of the Elastic Properties and Intrinsic Strength of Monolayer Graphene. *Science* **2008**, *321*, 385–388.
8. Kim, K. S.; Zhao, Y.; Jang, H.; Lee, S. Y.; Kim, J. M.; Kim, K. S.; Ahn, J. H.; Kim, P.; Choi, J. Y.; Hong, B. H. Large-Scale Pattern Growth of Graphene Films for Stretchable Transparent Electrodes. *Nature* **2009**, *457*, 706–710.
9. Ni, Z. H.; Yu, T.; Lu, Y. H.; Wang, Y. Y.; Feng, Y. P.; Shen, Z. X. Uniaxial Strain on Graphene: Raman Spectroscopy Study and Band-Gap Opening. *ACS Nano* **2008**, *2*, 2301–2305.
10. Lu, P.; Wu, X.; Guo, W.; Zeng, X. C. Strain-Dependent Electronic and Magnetic Properties of $MoS_2$ Monolayer, Bilayer, Nanoribbons and Nanotubes. *Phys. Chem. Chem. Phys.* **2012**, *14*, 13035–13040.
11. Wang, Q. H.; Kalantar-Zadeh, K.; Kis, A.; Coleman, J. N.; Strano, M. S. Electronics and Optoelectronics of Two-Dimensional Transition Metal Dichalcogenides. *Nat. Nanotechnol.* **2012**, *7*, 699–712.
12. Liu, K. K.; Zhang, W.; Lee, Y. H.; Lin, Y. C.; Chang, M. T.; Su, C. Y.; Chang, C. S.; Li, H.; Shi, Y.; Zhang, H.; *et al.* Growth of Large-Area and Highly Crystalline $MoS_2$ Thin Layers on Insulating Substrates. *Nano Lett.* **2012**, *12*, 1538–1544.
13. Zhang, Y.; Gao, G.; Chan, H. L. W.; Dai, J.; Wang, Y.; Hao, J. Piezo-Phototronic Effect-Induced Dual-Mode Light and Ultrasound Emissions from ZnS:Mn/PMN-PT Thin-Film Structures. *Adv. Mater.* **2012**, *24*, 1729–1735.
14. Zheng, R. K.; Wang, Y.; Wang, J.; Wong, K. S.; Chan, H. L. W.; Choy, C. L.; Luo, H. S. Tuning the Electrical Properties of $La_{0.75}Ca_{0.25}MnO_3$ Thin Films by Ferroelectric Polarization, Ferroelectric-Field Effect, and Converse Piezoelectric Effect. *Phys. Rev. B* **2006**, *74*, 094427–094433.
15. Rastelli, A.; Ding, F.; Plumhof, J. D.; Kumar, S.; Trotta, R.; Deneke, Ch.; Malachias, A.; Atkinson, P.; Zallo, E.; Zander, T.; *et al.* Controlling Quantum Dot Emission by Integration of Semiconductor Nanomembranes onto Piezoelectric Actuators. *Phys. Status Solidi B* **2012**, *249*, 687–696.
16. Lee, C.; Yan, H.; Brus, L. E.; Heinz, T. F.; Hone, J.; Ryu, S. Anomalous Lattice Vibrations of Single- and Few-Layer $MoS_2$. *ACS Nano* **2010**, *4*, 2695–2700.
17. Li, H.; Zhang, Q.; Yap, C. C. R.; Tay, B. K.; Teo, H. T. E.; Olivier, A.; Baillargeat, D. From Bulk to Monolayer $MoS_2$: Evolution of Raman Scattering. *Adv. Funct. Mater.* **2012**, *22*, 1385–1390.
18. Viršek, M.; Jesih, A.; Milošević, I.; Damnjanović, M.; Remskar, M. Raman Scattering of the $MoS_2$ and $WS_2$ Single Nanotubes. *Surf. Sci.* **2007**, *601*, 2868–2872.
19. Bagnall, A. G.; Liang, W. Y.; Marseglia, E. A.; Welber, B. Raman Studies of $MoS_2$ at High-Pressure. *Phys. B & C (Amsterdam, Neth.)* **1980**, *99*, 343–346.
20. Tongay, S.; Zhou, J.; Ataca, C.; Lo, K.; Matthews, T. S.; Li, J.; Grossman, J. C.; Wu, J. Thermally Driven Crossover from Indirect Toward Direct Bandgap in 2D Semiconductors: $MoSe_2$ *versus* $MoS_2$. *Nano Lett.* **2012**, *12*, 5576–5580.
21. Mak, K. F.; He, K.; Lee, C.; Lee, G. H.; Hone, J.; Heinz, T. F.; Shen, J. Tightly Bound Trions in Monolayer $MoS_2$. *Nat. Mater.* **2012**, *12*, 207–211.
22. Kwon, S. S.; Hong, W. K.; Jo, G.; Maeng, J.; Kim, T. W.; Song, S.; Lee, T. Piezoelectric Effect on the Electronic Transport Characteristics of ZnO Nanowire Field-Effect Transistors on Bent Flexible Substrates. *Adv. Mater.* **2008**, *20*, 4557–4562.
23. Ellis, J. K.; Lucero, M. J.; Scuseria, G. E. The Indirect to Direct Band Gap Transition in Multilayered $MoS_2$ as Predicted by Screened Hybrid Density Functional Theory. *Appl. Phys. Lett.* **2012**, *99*, 261908.
24. Scalise E.; Houssa, M.; Pourtois, G.; Afanasev, V. V.; Stesmans, A. First-Principles Study of Strained 2D $MoS_2$. *Phys. E (Amsterdam, Neth.)* **2013**, http://dx.doi.org/10.1016/j.physe.2012.07.029.
25. Mattheiss, L. F. Band Structures of Transition-Metal-Dichalcogenide Layer Compounds. *Phys. Rev. B* **1973**, *8*, 3719.
26. He, K.; Poole, C.; Mak, K. F.; Shan, J. Experimental Demonstration of Continuous Electronic Structure Tuning *via* Strain in Atomically Thin $MoS_2$. *Nano Lett.* **2013**, *13*, 2931–2936.
27. Peelaers, H.; Van de Walle, C. G. Effects of Strain on Band Structure and Effective Masses in $MoS_2$. *Phys. Rev. B* **2012**, *86*, 241401(R).
28. Conley, H.; Wang, B.; Ziegler, J.; Haglund, R. F.; Pantelides, S. T.; Bolotin, K. I. Bandgap Engineering of Strained Monolayer and Bilayer $MoS_2$. *Nano Lett.* **2013**, http://dx.doi.org/10.1021/nl4014748.
29. Liu, Q.; Li, L.; Li, Y.; Gao, Z.; Chen, Z.; Lu, J. Tuning Electronic Structure of Bilayer $MoS_2$ by Vertical Electric Field: A First-Principles Investigation. *J. Phys. Chem. C* **2012**, *116*, 21556–21562.
30. Zhou, Y.; Wang, Z.; Yang, P.; Zu, X.; Yang, L.; Sun, X.; Gao, F. Tensile Strain Switched Ferromagnetism in Layered $NbS_2$ and $NbSe_2$. *ACS Nano* **2012**, *6*, 9727–9736.
31. Pan, H.; Zhang, Y. W. Tuning the Electronic and Magnetic Properties of $MoS_2$ Nanoribbons by Strain Engineering. *J. Phys. Chem. C* **2012**, *116*, 11752–11757.
32. Kresse, G.; Furthmuller, J. Efficient Iterative Schemes for *Ab Initio* Total-Energy Calculations Using a Plane-Wave Basis Set. *Phys. Rev. B* **1996**, *54*, 11169–11186.
33. Kresse, G.; Hafner, J. *Ab Initio* Molecular Dynamics for Liquid Metals. *Phys. Rev. B* **1993**, *47*, 558–561.
34. Blöchl, P. E. Projector Augmented-Wave Method. *Phys. Rev. B* **1994**, *50*, 17953–17979.
35. Kresse, G.; Joubert, D. From Ultrasoft Pseudopotentials to the Projector Augmented-Wave Method. *Phys. Rev. B* **1999**, *59*, 1758–1775.
36. Perdew, J. P.; Burke, K.; Ernzerhof, M. Generalized Gradient Approximation Made Simple. *Phys. Rev. Lett.* **1996**, *77*, 3865–3868.
37. Baroni, S.; de Gironcoli, S.; Dal Corso, A.; Giannozzi, P. Phonons and Related Crystal Properties from Density-Functional Perturbation Theory. *Rev. Mod. Phys.* **2001**, *73*, 515–562.